Showcasing research from Professor Woodward's laboratory, GSK Carbon Neutral Laboratories for Sustainable Chemistry and School of Chemistry, University of Nottingham, United Kingdom.

Catalysis enabled synthesis, structures, and reactivities of fluorinated S_8-corona[*n*]arenes (*n* = 8–12)

Simple ammonium fluoride catalysts NR_4F (R = H, Me, *n*-Bu in pyridine) accelerate S_NAr reactions of C_6F_6 and related molecules, allowing the formation of the festive macrocycle shown in the graphic (Christmas red for the fluorines here!). Such large macrocycles can also be selectively *octa*-functionalised by thiols using the same catalysts, allowing rapid access to a wide range of molecular architectures and building blocks.

As featured in:

See Andrew. T. Turley, Simon Woodward *et al.*, *Chem. Sci.*, 2023, **14**, 70.

ROYAL SOCIETY OF CHEMISTRY

rsc.li/chemical-science

Registered charity number: 207890

Chemical Science

ROYAL SOCIETY OF CHEMISTRY

EDGE ARTICLE

View Article Online
View Journal | View Issue

Cite this: *Chem. Sci.*, 2023, **14**, 70

All publication charges for this article have been paid for by the Royal Society of Chemistry

Catalysis enabled synthesis, structures, and reactivities of fluorinated S_8-corona[*n*]arenes (*n* = 8–12)†

Andrew. T. Turley, *[a] Magnus W. D. Hanson-Heine, [b] Stephen. P. Argent, [b] Yaoyang Hu, [a] Thomas. A. Jones, [a] Michael Fay [c] and Simon Woodward *[a]

Received 25th September 2022
Accepted 13th November 2022

DOI: 10.1039/d2sc05348a

rsc.li/chemical-science

Previously inaccessible large S_8-corona[*n*]arene macrocycles (*n* = 8–12) with alternating aryl and 1,4-C_6F_4 subunits are easily prepared on up to gram scales, without the need for chromatography (up to 45% yield, 10 different examples) through new high acceleration S_NAr substitution protocols (catalytic NR_4F in pyridine, R = H, Me, Bu). Macrocycle size and functionality are tunable by precursor and catalyst selection. Equivalent simple NR_4F catalysis allows facile late-stage S_NAr difunctionalisation of the ring C_6F_4 units with thiols (8 derivatives, typically 95+% yields) providing two-step access to highly functionalised fluoromacrocycle libraries. Macrocycle host binding supports fluoroaryl catalytic activation through contact ion pair binding of NR_4F and solvent inclusion. In the solid-state, solvent inclusion also intimately controls macrocycle conformation and fluorine–fluorine interactions leading to spontaneous self-assembly into infinite columns with honeycomb-like lattices.

Introduction

Accessing functionalised macrocyclic molecules with well-defined cavities is a major focus in supramolecular chemistry due to their synthetic challenge, unique shapes, and selective guest binding abilities.[1–3] Such characteristics are vital in chemical sensing,[4,5] drug delivery,[6] self-healing materials,[7] catalysis,[8] and molecular electronic applications,[9] and more generally, when (self)assembling any complex supramolecular architecture.[10] Outside cycloamides and cyclodextrins, easily accessed macrocycles capable of single-step functionalisation are remarkably rare.[2] For example, while aryl-rich macrocycles abound, *e.g.* pillar[*n*]arenes,[11–13] calix[*n*]arenes,[14–17] and corona[*n*]arenes;[18,19] installing suitable functional handles within these is typically time-consuming and problematic (Fig. 1a) and this prevents rapid access to onward functionality diversification.[20–24] For such cases derivatisation is required, leading to longer synthetic routes, reduced overall efficiency and time-consuming chromatographic separations of multiple intermediates. Potentially, catalytic macrocyclisation of commercial C_6F_6 (or a simple analogue thereof) offers an elegant solution to such problems, as both the macrocyclisation and subsequent derivatisation can potentially be achieved by simple C–F displacements in single-step reactions. The

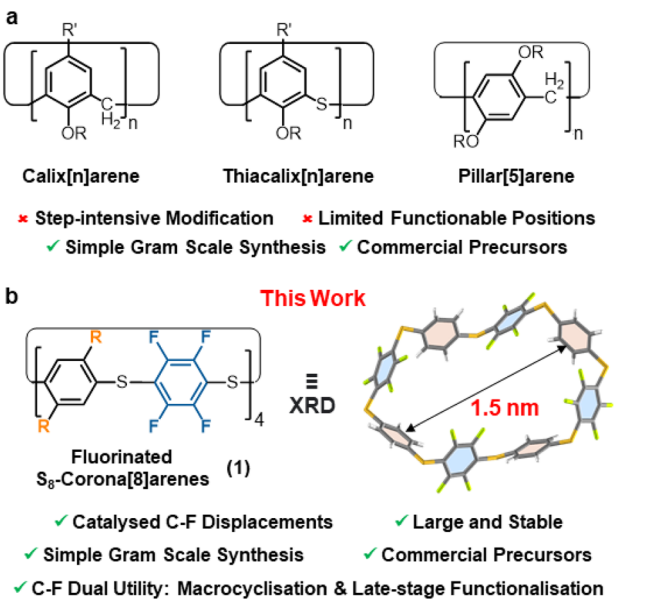

Fig. 1 (a) Widely used, but harder to functionalise, arene macrocycles. (b) A typical S_8-corona[8]arene (**1a**, R = H) with catalyst labile C–F motifs for new one-step synthesis and late-stage catalytic functionalisation.

[a]*GSK Carbon Neutral Laboratories for Sustainable Chemistry, University of Nottingham, Jubilee Campus, Nottingham NG7 2TU, UK. E-mail: andrew.turley@nottingham.ac.uk; simon.woodward@nottingham.ac.uk*

[b]*School of Chemistry, University of Nottingham, University Park Campus, Nottingham NG7 2RD, UK*

[c]*Nanoscale and Microscale Research Centre, University of Nottingham, University Park Campus, Cripps South Building, Nottingham, NG7 2RD, UK*

† Electronic supplementary information (ESI) available: Full experimental and characterisation data. Primary kinetic and guest binding data (Excel format). CCDC 2175101–2175106. For ESI and crystallographic data in CIF or other electronic format see DOI: https://doi.org/10.1039/d2sc05348a

resultant novel fluorinated macrocycles would offer significant advantages over their non-fluorinated forbearers.[25]

Herein, we report one-pot catalytic protocols using C_6F_6 (and analogues) to form the robust, fluorinated macrocycle S_8-corona[8]arene **1a** (R = H) and its derivatives (Fig. 1b), whereby the C–F bonds are rapidly displaced in new templated catalytic macrocyclisation approaches and late-stage functionalisations. Highly catalyst accelerated S_NAr substitutions of perfluoroaryl units enable these new mechanism driven protocols.‡

The aryl macrocycles (**1**) are prepared from low cost materials on up to gram scales in 1–3 steps without any special conditions. Purification is achieved without the need for chromatographic separations or recrystallisation. Instead, all the macrocycles reported here are isolated simply by filtering off any insoluble by-products formed. To the best of our knowledge, this is the first report of readily accessible corona[*n*]arenes with $n > 6$,[19] and the first to realise one-step aryl functionalisation. The reactions are general and libraries of S_8-corona[*n*]arene (**1**) derivatives with varying symmetries and substitution patterns are readily attained. Catalytic functionalisation of the derived S_8-corona[*n*]arenes (**1**) themselves with thiols is also rapid at room temperature, allowing further highly diverse functional fluorinated macrocycles to be attained in just two steps. Additionally, the solvent and ammonium guest binding behaviour of **1** is in accord with the new NR_4F/pyridine C–F activation protocol proposed and demonstrates the wide potential of S_8-corona[*n*]arenes (**1**) in host-guest applications.

Results and discussion

Macrocyclisation of C_6F_6 in the presence of dinucleophiles is inordinately challenging due to competing linear oligomerisation. Previous attempts have ended only in polymer production.[26] Our own initial trials, using commercial C_6F_6 and benzene-1,4-dithiol (**2a**,§ Scheme 1a), under a variety of classical S_NAr conditions, also just provided an insoluble polymer (**P1**, ESI Fig. S221–S225† for polymer data). Thus, we sought a new S_NAr protocol offering both high rate S_NAr acceleration but also the templating needed to favour macrocycle (**1**) formation. Screening revealed ammonium fluoride catalysts in pyridine to be particularly effective‡ while more traditional S_NAr solvents vastly favoured polymerisation. When NH_4F (**AF**), NMe_4F (**TMAF**), and NBu_4F (**TBAF**) are used as catalytic-base-templates in pyridine, the reaction between **2a** and C_6F_6 immediately provides appreciable amounts of macrocycle **1a** (Scheme 1a). To the best of our knowledge, this is the first example of use of ammonium fluorides as a dual-function catalytic-base-templates in one reaction. Catalyst loadings of 1 mol% give equivalent production of **1a** and reactions at 0.1 mol% are still practical. Control studies with other NR_4X (R = Me, Bu; X = Cl, Br, I) promotors, even in stoichiometric amounts, did not yield any **1a**, only polymer (**P1**) and unreacted starting materials are observed by ^1H and ^{19}F NMR spectroscopy in these control reactions. DFT studies (ESI Fig. S216† for full calculation details) indicate an unusual $C_6F_6\cdots NMe_4F$ ion pair association mode that increases the sp^3 character of the fluoroaryl carbons (weaker C=C character). This is the likely origin of the remarkable S_NAr acceleration observed (ESI Fig. S213–S215† and data for kinetic simulation of **1a** formation). This is in addition to the macrocyclisation effects of the same NR_4F template-catalysts. The use of pyridine is important as this solvent particularly favours the formation of the necessary NR_4F contact ion pairs.[27]

Optimisation provided a one-pot preparation of macrocycle **1a** in moderate, but practical and scalable yields, through the 10 min addition of C_6F_6 to a vigorously stirred 0.05 M solution of **2a**,§ in pyridine containing 5 mol% **TMAF** at room temperature (Scheme 1a). All starting materials and active intermediates are fully consumed, providing S_8-corona[8]arene (**1a**) and minor amounts of the larger S_{12}-corona[12]arene **1a′** (**1a** : **1a′** = 88 : 12) along with some acyclic/cyclic oligomers and insoluble polymer **P1**. Purification of this mixture is straightforward: **P1** is simply removed by filtration once the reaction is completed, leaving only the macrocycles and trace non-macrocyclic materials in the

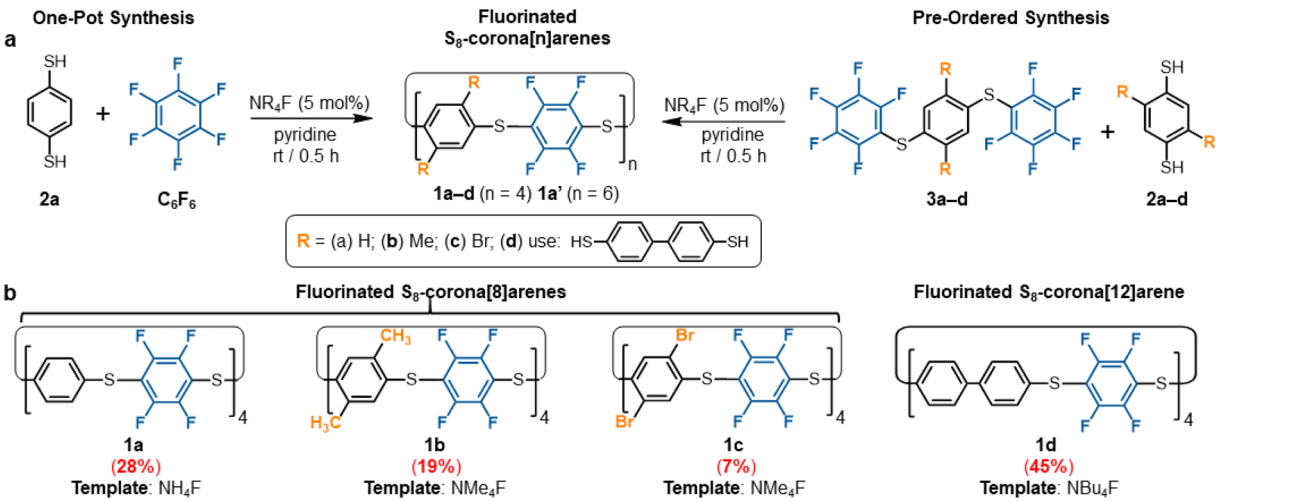

Scheme 1 (a) Two routes to synthesise fluorinated S_8-corona[*n*]arenes (**1**): from C_6F_6 and from analogues (**3**). (b) Schematic representations of macrocycles (**1a–d**) synthesised from the pre-ordered route, indicating the optimal NR_4F catalytic template.

solution. Trituration of the soluble fraction with pentanes removes all non-macrocyclic material, affording a colourless crystalline solid of **1a** and **1a′** in a 27–31% yield. Both **1a** and **1a′** show singlets in their ^{1}H (Fig. 2) and ^{19}F NMR spectra with similar chemical shifts.

MALDI-TOF mass spectrometry confirmed the identity of both macrocycles showing the expected mass and S_8/S_{12} isotope patterns (ESI Fig. S134–S138†). Only negligible change in the relative ratios of **1a** and **1a′** is observed in the one-pot reaction as a function of catalyst (compared to the fragment **3a** approach below). Diffusion-Ordered NMR Spectroscopy (DOSY) was employed to distinguish the peaks correlating to **1a** and **1a′**, confirming the major product as **1a** (Fig. 2b). Analytically pure **1a** can be obtained through sublimation (0.9 mbar, 300–350 °C) of the **1a** and **1a′** mixture.

Pre-ordered synthesis of S_8-corona[8]arene (1a)

To attain **1a** chemospecifically, we devised a 'pre-ordered' approach, replacing C_6F_6 with thioether **3a** (which is easily synthesised in high yields over two steps without extensive purification§). Use of **3a** and a NH_4F catalyst affords **1a** chemospecifically (no. S12-corona[12]arene **1a′**, Fig. 2a), on gram scales, without the need for chromatography, in a 28% yield (Scheme 1b). Even allowing for the initial preparation of **3a**, gram amounts of **1a** can be obtained rapidly without extensive purification requirements (24% yield over 3 steps). Again, only insoluble polymeric material results in the absence of the ammonium fluoride catalytic template. When using **3a** (compared to C_6F_6) the choice of ammonium fluoride catalyst has a direct influence on the ratio of **1a** to **1a′** (Fig. 2a). As might be anticipated, larger ammonium fluoride templates favour **1a′**. While NH_4F (**AF**) catalyses the formation of only **1a** chemospecifically (Fig. 2a, **1a** : **1a′** ratio 1 : 0.00), as the size of the catalytic template increases the amount of **1a′** also increases (up to a **1a** : **1a′** ratio of 1 : 0.15 for **TBAF**). However, in each instance, the macrocycle yields remain comparable and DOSY NMR confirms only **1a** and **1a′** form (Fig. 2b).

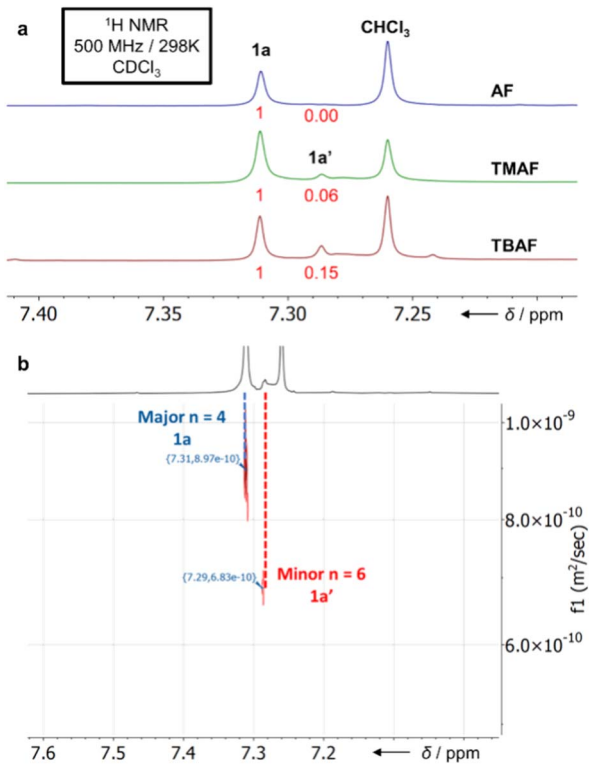

Fig. 2 Partial (a) ^{1}H NMR spectra ($CDCl_3$) of S_8-corona[8]arene (**1a**) and S_{12}-corona[12]arene (**1a′**) as synthesised *via* **3a** promoted by different ammonium fluoride catalysts. (b) Diffusion-Ordered Spectroscopy (DOSY) NMR spectrum of a **1a** : **1a′** mixture.

S_8-Corona[8]arene (1b–d and 1ab–cd) library synthesis

The scope of the chemoselective macrocyclisation procedure was investigated using a range of easily prepared benzene-1,4-dithiols (**2b–d**) and thioether linkers (**3b–d**).§ With **TMAF** catalysis macrocycles **1b–d** are synthesised chemoselectively as the desired S_8-corona[*n*]arenes in a range of yields (7–45%). DFT calculations revealed a negligible difference in the $C^{\delta+}$–$F^{\delta-}$ polarisation energies (natural atomic charges) at the point of substitution within **3**, yet significant differences in the rotational energy barrier (from 0.2 to 5.9 kcal mol^{-1}) for S–C_6F_5 bond rotation of the terminal fluorobenzenoids in the thioethers (**3b** > **3c** > **3a** > **3d**) (ESI Scheme S4 and Table S4†). As expected, increase in the steric demands of **3b** and **3c** compared to **3a** results in lower yields of the corresponding macrocycles. Conversely, reducing the steric constraints by employing a 1,1′-biphenyl linker leads to the S_8-corona[12]arene (**1d**) in higher yield (45%) although an appropriate (larger) **TBAF** catalytic template is needed. Using pairs of different **2a–d** and **3a–d** linkers allows rapid access to the library of dissymmetric S_8-corona[*n*]arenes **1ab–cd** chemoselectively (Fig. 3). As anticipated, some combinations of **2** and **3** are higher-yielding than others, which is attributed to the steric hindrance associated with the final macrocycle, and the rotational barrier of linkers **3a–d** as previously discussed. Additionally, Fig. 3 shows the importance of pairing the nucleophile and electrophile combinations appropriately. The clearest example of this is the synthesis of **1bc** (yields in red). A combination of the high rotational barrier linker **3b** and low nucleophilicity 1,4-dithiol **2c**, provides no macrocycle at all and only insoluble polymeric materials (92% by mass) and unreacted **3b** (8% by mass) are recovered. Using instead the matched combination of **2b** and **3c** (simultaneously increasing nucleophile and electrophile reactivity) realises **1bc** in modest yield. The poor nucleophilicity of **2c**, can also be overcome with linker **3d**, which has reduced rotational barriers allowing access to the large tetrabromide S_8-corona[10]arene, **1cd** in improved (32%) yield. In most cases of **1**, the 8-ring S_8-corona[*n*]arene framework forms highly chemoselectively, the exceptions being **1ab** and **1bc** where both the corresponding S_8-corona[8]arene and S_{12}-corona[12]arene are formed (independent of the precursor combination or catalyst used). Proton NMR analysis provides a [8] : [12] ratio of 1 : 0.13 for **1ab** and 1 : 0.33 for **1bc** respectively, with the smaller, S_8-corona[8]arene being the major product for both (ESI Fig. S41, S81, and S132–S133†). DOSY/2D NMR spectroscopy (ESI Fig. S39–S133†) and MALDI-TOF mass spectrometry (ESI

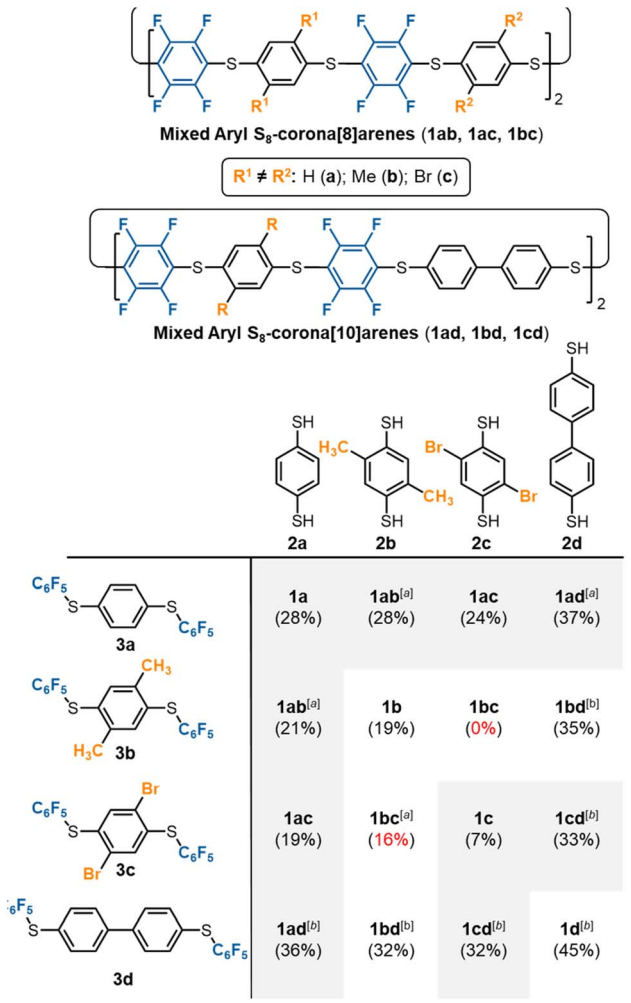

Fig. 3 Library synthesis of mixed S_8-corona[*n*]arenes (**1**). Footnotes: [a] mixture of both S_8 (*n* = 2, major) and S_{12} (*n* = 3, minor) **1** formed; [b] TBAF used as catalyst instead of TMAF.

Fig. S134–S175†) confirm the preparation of all ten new S_8-corona[*n*]arenes. In particular, each macrocycle shows a clear S_8 isotope pattern at the expected mass, while the dissymmetric mixed aryl systems **1ab–cd** show two ^{19}F NMR environments as 'AB' systems or overlapping multiplets at *ca.* −133.0 ppm.

Solid state structure

Single crystals of **1a**, suitable for X-ray diffraction, are obtained by either slow evaporation or solvent layering confirming the connectivity and size of **1a** (see ESI† for full crystallographic details, ESI Fig. S139–S211† and cif files). We identified five solvates of **1a** (**1a**–hexane, **1a**–$CHCl_3$, **1a**–THF, **1a**–pyridine and **1a**–DMF). Three instructive examples are shown here (Fig. 4). While all pack in infinite honeycomb-like channels each solvate exhibits a dramatically different solid-state macrocyclic conformation. That in **1a**–hexane (Fig. 4a) has an open crown-like conformation where the average C–S–C bond angle is 101.46°. The internal cavity of **1a**–hexane, measured between centroids of opposite aryl units, has a large semi-major axis of 1.46 nm, is absent of ordered solvent and any intramolecular interactions distorting the internal cavity. Its solid-state structure differs from conventional 'pillar-like' arene macrocycles[12] and instead, the arene units tilt alternatingly. To elucidate the important non-covalent interactions in the one-dimensionally assembled **1a**–hexane macrocycles, Hirschfield analysis[28] was employed (ESI Fig. S196†). Intermolecular hydrogen bonding (H–F contacts), type 1 F–F, and F–CH interactions between neighbouring aryl units (above and below) were identified as the major interactions dictating the columnar self-assembly of **1a**–hexane (Fig. 4a). Between columns, intermolecular interactions between adjacent C_6H_4 units, 3 × CH–π (2.73 Å), and adjacent C_6F_4 units 4 × CF–π (2.96 Å) and 1 × F–F (2.77 Å) are present and dictate the adoption of the three-dimensional honeycomb-like lattice.

When crystallised from $CHCl_3$, **1a** forms a solid-state 1 : 2 host–guest inclusion complex, **1a**⊂2$CHCl_3$ (Fig. 4b). The macrocycle within this **1a**–$CHCl_3$ solvate adopts a 'staircase-like' conformation where the individual aryl units now point face-inwards to maximise electrostatic interactions between **1a** and the guest. To efficiently accommodate both guests, the macrocycle lengthens to 1.57 nm, with an 8.40 Å reduction in width, and an increase in the average C–S–C bond angle to 103.51°, forming two equal and symmetrical binding sites on opposite sides of the macrocycle, to minimise unfavourable interactions between guests. This same conformational shift, in response to guest binding, is also observed in related **1a**–THF, where a similar staircase-like conformation arises in response to a 1 : 2 host–solvent complex. While disorder prevents exact THF detection, the staircase conformation explicitly points to it. After 1 : 2 guest binding, the columnar supramolecular packing of **1a** remains, generating infinite rigid column arrays (dictated by intermolecular hydrogen bonding between adjacent C_6H_4 and C_6F_4 units) saturated with guest/solvent molecules, a feature that is highly sought after for many applications, for example, gas exchange materials.[29]

When single crystals of **1a** are grown through slow evaporation of DMF solutions, the macrocycle adopts a 'tub-like' conformation reminiscent of cyclooctatetraene (**1a**–DMF, Fig. 4c). Unlike with **1a**–$CHCl_3$, here the DMF solvent remains disordered amongst sheets of **1a** in the solid state. The asymmetric unit reveals a pair of **1a** macrocycles stacked on top of each other, with each C_6H_4 stacking on to a proximal C_6F_4 unit (and *vice versa*) to maximise intermolecular hydrogen bonding between adjacent macrocycles. As in the other structures, these weak hydrogen bonds facilitate the formation of well-defined columns, which are characteristic of all the solvates of **1a** identified to date. Substitution of R = H (**1a**) to other macrocycles changes this behaviour. For example, in the X-ray structure of **1b** (R = Me, ESI Fig. S209†) staggered channels form with overlap between adjacent columns, forming infinite chain-linked columns, permitting multiple intermolecular CF–π interactions to form (ESI Fig. S210†).

Late-stage library functionalisation

All the S_8-corona[*n*]arene backbones (**1**), reported here, can be used as versatile macrocyclic backbones for one-step late-stage

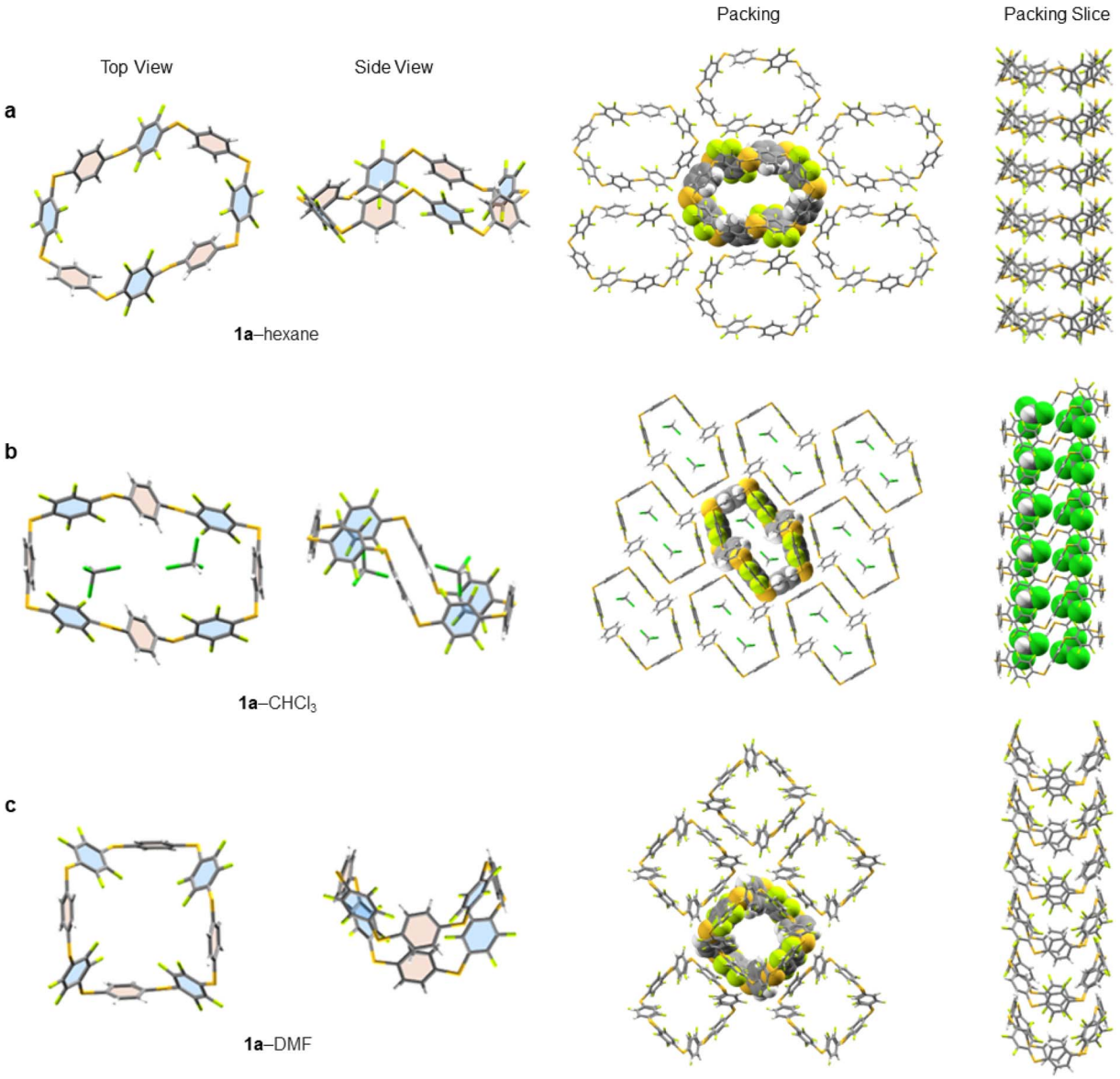

Fig. 4 X-ray solid-state structures of **1a** crystallised from: (a) hexane (b) $CHCl_3$ and (c) DMF, viewed from the top and side. The solid-state packing of each crystal is viewed from the top and side where a central molecule or guest (space-filling representation) is shown embedded in a section of the lattice to illustrate the unidirectional crystal packing. All disordered solvent is removed for clarity, leaving highly ordered $CHCl_3$ (part b of figure) to demonstrate the role of solvent in the final solid-state conformation of **1a**.

S_NAr-based multi-functionalisations, rapidly and selectively without recourse to multi-step protecting group strategies. They provide excellent building blocks for a wide range of onwards chemistries. This is an important feature for convenient adoption and provides an alternative macrocyclic framework to current air-sensitive hydroxypillarene approaches.[23]

As a proof-of-concept, our **TMAF**/pyridine S_NAr catalysis protocol was used to synthesise a range of thiol substituted S_8-corona[*n*]arenes under mild conditions in high yields (Scheme 2). In each case, these substitutions converge into a single isomerically pure product, overcoming the need for laborious separations of positional isomers. The large aryl thiol units along with the steric restraints of the macrocycle framework prevent complete substitution of all 16 aryl-fluoride groups within **1a**. Instead, only selective 2,5-functionalisation occurs on every C_6F_4 unit for a total of 8 substitutions. Initial testing was conducted on NMR scales with a small excesses of thiophenol (10–16 equiv.) being added to a sample of **1a** in pyridine containing **TMAF** with no precautions taken to remove oxygen or moisture: ^{19}F NMR analysis shows the singlet at −134 ppm for **1a** is quickly disrupted into many peaks spanning −90 to −134 ppm which are attributed to the positional isomers caused by partial substitutions. Over the course of 2 hours, these peaks all converge into a new singlet at *ca.* −90 ppm, representing the targeted 2,5-functionalised macrocycle **4a** (ESI Fig. S129† for NMR monitoring). Macrocycles **1b** and **1d**, show equal success in equivalent functionalisation with thiophenol. In all cases, purification is straightforward with simple

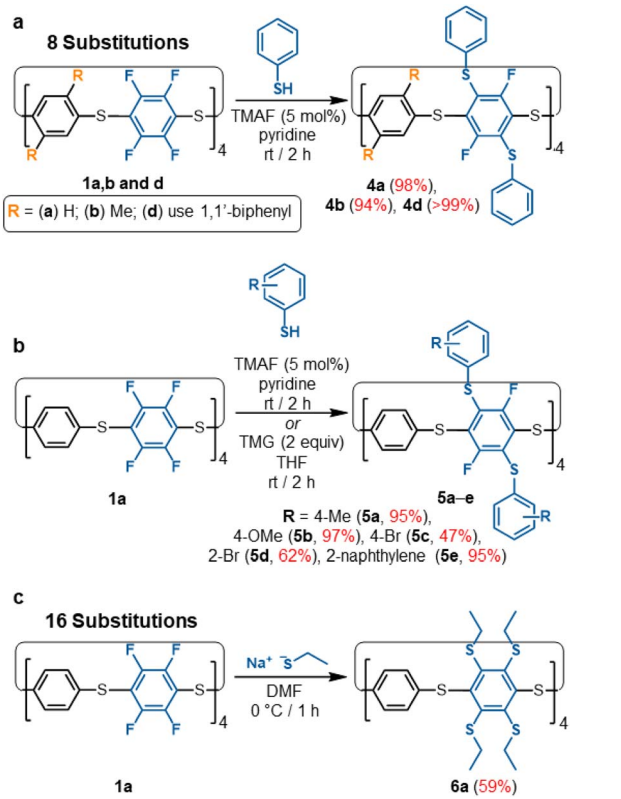

Scheme 2 (a) Synthesis of thiophenol functionalised S_8-corona[*n*]arenes (**4a**, **4b**, **4d**). (b) Scope of 8-fold functionalisation of **1a** to **5a–e**; (c) 16-fold functionalisation of **1a** to **6a**.

trituration with water, MeOH, and then Et_2O (to remove pyridine HF-pyridine, **TMAF**, unreacted excess nucleophile, and any disulfide) being sufficient to isolate **4** as pure colourless solids. The [8SPh]S_8-corona[*n*]arenes (**4a**, **4b**, and **4d**) are equivalently attained in excellent yields, selectively, in a single step from **1a**, **1b**, and **1d** respectively (Scheme 2a). To confirm equivalent reactivity at scale, **4a** was synthesised under the same conditions on a *ca.* 0.1 g scale and successfully isolated in 98% yield. Numerous thiophenol derivatives also readily participate of which **5a–5e** provide a representative series. In all cases the catalysed S_NAr reactions converge into a single octafunctionalised derivative in fair to excellent yields without the need for large excesses of thiol.

Attempted complete C–F displacement of **1a** using large excesses of PhSH and heating results in significant thiol–thioether exchange causing the macrocyclic framework to break down into an uncharacterisable mixture. However, per-substitution of **1a** could be achieved using smaller, non-aryl nucleophiles such as sodium ethanethiolate, providing **6a** under mild conditions (Scheme 2c). Restricted rotation barriers result in broad ^{1}H NMR signals (ESI Fig. S124†) and prevent ^{13}C NMR characterisation. However, the absence of ^{19}F NMR signals and a clear MALDI-TOF molecular ion confirm per-substituted (ESI Fig. S191–S192†). With their ease of substitution and convenient ^{19}F NMR handle for reaction monitoring, S_8-corona[*n*]arene backbones **1** are, we propose, highly attractive versatile building blocks for wide fields of application, *e.g.* 'designer' guests, molecular machine components, organic frameworks, *etc.*

Host–guest binding studies

Next, we turned to UV-vis titration experiments of **1a** in THF solution with a variety of guests relevant to our catalytic, synthetic and X-ray studies to determine their binding affinities/energetics (ESI Fig. S212† and provided data). Due to the high THF (neat) solvent molecularity (12.3 M), titration of small amounts of alternate guests (G) into THF solutions of **1a** (entropically) favours 1 : 1 binding, provided no cooperative guest binding effects occur.[30] When 10 μM solutions of **1a** in THF are titrated with $CHCl_3$, DMF, and pyridine these provide reproducible good fits to 1 : 1 binding isotherms, based on simulation of the absorbance maxima at 295 nm (Table 1). Binding of larger NBu_4Cl follows the same 1 : 1 behaviour, as does NBu_4F, provided low relative concentrations (**1a** : NBu_4F < 1 : 5) of the latter guest are used. At higher relative concentrations of NBu_4F : **1a** a second association process is triggered and a new charge transfer band ($\varepsilon_{HG} = 5.9(9) \times 10^4$ M^{-1} cm^{-1}) at 370 nm, associated with a clear isosbestic point at *ca.* 315 nm, appears. These indicate the presence of a second species whose formation is induced by the initial NBu_4F binding. A second 1 : 1 binding constant of $K = 1.0(3) \times 10^3$ M^{-1} (R^2 0.97) can be determined from absorbance data at 370 nm indicating this second process has $\Delta G°$ −4.0 kcal mol^{-1}. This value is rather close to the gas-phase association energy we determine (DFT) for the interaction of NMe_4F with C_6F_6 (−12 kcal mol^{-1}, ESI Fig. S216†). We therefore propose that the charge transfer band at 370 nm is direct experimental evidence for the $NR_4F\cdots$fluoroaryl interaction we calculate (ESI Fig. S216†), and that this is at the heart of the high S_NAr rate accelerations we see in the formation of **1a** and in its subsequent derivatisations.

Control studies indicate that the absorbance of **1a** in THF is only weakly affected by the presence of water (δ_{Abs} 0.001–0.003), when the water levels in the THF are 150–250 ppm. All our studies were conducted at 190 ± 20 ppm water in THF as measured by Karl–Fisher titration. Water concentrations, above 300 ppm negatively affect the initial 1 : 1 guest binding (*c.f.* the DMF guest entry data within Table 1). This is most acutely apparent in attempted determinations of NMe_4F binding to **1a**.

Table 1 1 : 1 Guest binding to macrocycle **1a**[a]

Guest	K (M^{-1})	ε_{HG} (M^{-1} cm^{-1})	$\Delta G°$ (kcal mol^{-1})	(R^2)
$CHCl_3$	3.6(7)	$5.85(10) \times 10^4$	−0.8	0.99
DMF	7.4(8)[b]	$5.56(4) \times 10^4$	−1.2	0.99
Pyridine	$8(1) \times 10^3$	$5.7(3) \times 10^4$	−5.2	0.97
NBu_4Cl	$2.6(3) \times 10^4$	$6.14(4) \times 10^4$	−5.9	0.98
NBu_4F	$1.5(2) \times 10^4$	$7.15(10) \times 10^4$	−5.6	0.99

[a] Determined by UV-vis titration in THF containing 190 ± 20 ppm water; the average of two reproducible duplicates is presented. The number in parentheses indicates the standard deviation in the preceding figure. [b] $K = 3.3(6)$ M^{-1} (R^2 098) in THF containing 300 ppm water.

Hydrated NMe_4F is insoluble in THF and only readily soluble in DMF containing significant water (*ca.* 2000 ppm). This water reduces NMe_4F binding to **1a** to a point where reproducible accurate *K* values cannot be determined. However, it is still clear from the qualitative UV spectra that the same two-step process is occurring, as the same 370 nm charge transfer band still emerges at higher **1a** : NMe_4F ratios. It is likely, based on our X-ray data, that initial guest binding to macrocycle **1a** is driven by H-bonding and π–π interaction, while the second association of additional NR_4F involves interaction of a C_6F_4 unit within **1a** with a NR_4F contact ion pair (DFT calculated, ESI Fig. S216†). To test this hypothesis, NMe_4F binding to **1a** was attempted in dry $THF/CH_2Cl_2/MeOH$ mixtures. The presence of MeOH is known to deliver the solvent separated ion pair $NMe_4^+ F^-$.[27] Consistent with our proposal, no binding of any type of **1a** to NMe_4F is observed in this solvent mixture.

To help identify the solution state conformation of **1a** a DFT conformational search was also made (ESI Fig. S217†). In the absence of guests, the lowest energy conformers are associated with transannular π–π contacts of the two central phenylene rings (either $C_6F_4\cdots C_6F_4$, or $C_6H_4\cdots C_6H_4$, see ESI Fig. S217†). These structures are significantly lower in energy than the open conformation of unsolvated **1a** (as modelled from the X-ray structure of **1a**-hexane). In adopting such π–π stacked conformers the macrocycle **1a** twists generating two independent 'bays', each suitable for independent binding of a single guest. This arrangement is rather similar to that observed in the X-ray crystal structure of **1a**–$CHCl_3$, minus its guests. The $S_0 \rightarrow S_n$ absorption spectra of the two calculated lowest energy conformers (in the absence of any guest) using adiabatic linear-response time-dependent density functional theory (TDDFT) with the M06-2X/6-311++G(d,p) functional and electronic basis set combination are in accord with the experimental solution spectra (250–300 nm). Conversely, the charge transfer band (370 nm) observed with NR_4F (R = Me, Bu) is most consistent with a $NR_4FC_6F_n$ ($n = 4$–6) contact lowering the C=C bond order of the fluoroaryl unit.

Conclusions

New S_NAr catalytic-template protocols using NR_4F (R = H, Me, Bu) in pyridine allow unprecedented access to large fluorinated S_8-corona[*n*]arenes **1** ($n = 8$, 10, 12). This new class of functional sulphur-bridged arene macrocycle is easily and rapidly prepared from low cost and widely available reagents. Yields approaching 45% and preparations at gram scales (without recourse to tedious chromatographic separation) are readily attained in technically simple reactions. Kinetic, thermodynamic and computational studies are in accord with catalytic activation arising from fluoroaryl$\cdots NR_4F$ ion pair binding delivering rate acceleration and macrocyclic templating. Importantly, the pyridine solvent favours the necessary ion pairs,[27] but also binds the product macrocycle sufficiently well ($K \sim 8 \times 10^3$ M^{-1}) that it is calculated to displace the catalyst from **1** (when present in excess) allowing catalytic turn over. An additional benefit of fluorinated S_8-corona[8]arenes **1** is their predisposition to efficient and highly selective S_NAr C_6F_4-sub unit substitution reactions with thiols using the same NR_4F catalysis protocols. Entirely regiospecific eight-fold substitutions in nearly quantitative yields are attained without the need for large excesses of thiol. Overall, the excellent hosting and easy 'designer' potential of **1** gives this new class of macrocycle very high potential for use across the molecular, supramolecular and polymeric sciences in many applications, especially as they are so easily prepared.

Data availability

All available primary data are provided in the main text and ESI.†

Author contributions

A. T. T. synthesised and characterised all materials. M. W. D. H.-H. performed DFT calculations and simulations. S. P. A. collected and resolved all crystallographic data. M. F. coordinated SEM studies and analysis. Y. H. collected SEM data for **1a** and **P1**. S. W. carried out the kinetic and thermodynamic studies. A. T. T. and S. W. co-wrote the manuscript and conceived the research. All authors have reviewed and given approval to the final version of the manuscript.

Conflicts of interest

The macrocycle **1a** is now commercially available from **https://www.keyorganics.net**, A. T. T and S. W. declare their interest in this venture.

Acknowledgements

A. T. T. and S. W. acknowledge the support of a Leverhulme Trust Project Grant (RPG-2018-331). M. W. D. H.-H. acknowledges the University of Nottingham Green Chemicals Beacon. Y. Hu acknowledges support through the University of Nottingham Propulsion Futures Beacon and the EPSRC (EP/V047256/1). We acknowledge Diamond Light source for time on Beamline I19 under proposal CY21755. We are grateful to Dr Jeremy Titman for his assistance with preliminary solid-state NMR measurements.

Notes and references

‡ Catalysed S_NAr substitutions using simple acyclic models of the sub-units within **1** also complete within minutes (compared to hours for the control uncatalysed reactions). Thus, the rate acceleration observed for NR_4F/pyridine is in addition to any global ring templating effects (ESI Fig. S215†).

§ Commercial **2a–d** are also easily obtained at a low cost from the 2–3 step chromatography-free procedures outlined in the ESI.† The same is true for fragments **3a–d**.

1 J.-M. Lehn, *Angew. Chem., Int. Ed. Engl.*, 1988, **27**, 89.
2 A. Blanco-Gómez, P. Cortón, L. Barravecchia, I. Neira, E. Pazos, C. Peinador and M. D. García, *Chem. Soc. Rev.*, 2020, **49**, 3834.
3 J. Yu, D. Qi and J. Li, *Commun. Chem.*, 2020, **3**, 1.

4 R. Pinalli, A. Pedrini and E. Dalcanale, *Chem. Soc. Rev.*, 2018, **47**, 7006.
5 H. M. Tay and P. Beer, *Org. Biomol. Chem.*, 2021, **19**, 4652.
6 J. Chen, Y. Zhang, L. Zhao, Y. Zhang, L. Chen, M. Ma, X. Du, Z. Meng, C. Li and Q. Meng, *ACS Appl. Mater. Interfaces*, 2021, **13**, 53564.
7 Y. Wang, Y. Sun, A.-J. Avestro, P. R. Mcgonigal and H. Zhang, *Chem*, 2022, **2**, 480.
8 D. Kauerhof and J. Niemeyer, *ChemPlusChem*, 2020, 889.
9 H. Chen and J. F. Stoddart, *Nat. Rev. Mater.*, 2021, **6**, 804.
10 *Handbook of Macrocyclic Supramolecular Assembly*, ed. Y. Liu, Y. Chen and H.-Y. Zhang, Springer, Singapore, 2020.
11 T. Ogoshi, T. A. Yamagishi and Y. Nakamoto, *Chem. Rev.*, 2016, **116**, 7937.
12 M. Xue, Y. Yang, X. Chi, Z. Zhang and F. Huang, *Acc. Chem. Res.*, 2012, **45**, 1294.
13 T. Ogoshi, S. Kanai, S. Fujinami, T. A. Yamagishi and Y. Nakamoto, *J. Am. Chem. Soc.*, 2008, **130**, 5022.
14 V. Böhmer, *Angew. Chem., Int. Ed. Engl.*, 1995, **34**, 713.
15 S. Abi Fayssal, T. Naret, J. Buendia, A. Labattut, V. Huc, C. Martini and E. Schulz, *Adv. Synth. Catal.*, 2022, **364**, 947.
16 V. Guérineau, M. Rollet, S. Viel, B. Lepoittevin, L. Costa, P. Saint-Aguet, R. Laurent, P. Roger, D. Gigmes, C. Martini and V. Huc, *Nat. Commun.*, 2019, **10**, 1.
17 O. Santoro and C. Redshaw, *Coord. Chem. Rev.*, 2021, **448**, 214173.
18 S. Y. Zhuang, Y. Cheng, Q. Zhang, S. Tong and M. X. Wang, *Angew. Chem., Int. Ed.*, 2020, **59**, 23716.
19 M. Y. Zhao, D. X. Wang and M. X. Wang, *J. Org. Chem.*, 2018, **83**, 1502.
20 N. L. Strutt, H. Zhang, S. T. Schneebeli and J. F. Stoddart, *Acc. Chem. Res.*, 2014, **47**, 21.
21 Z. Li and Y.-W. Yang, *Acc. Mater. Res.*, 2021, **2**, 292.
22 Y. Chao, T. U. Thikekar, W. Fang, R. Chang, J. Xu, N. Ouyang, J. Xu, Y. Gao, M. Guo, H. Zuilhof and A. C.-H. Sue, *Angew. Chem., Int. Ed.*, 2022, e202204589.
23 P. Demay-Drouhard, K. Du, K. Samanta, X. Wan, W. Yang, R. Srinivasan, A. C.-H. Sue and H. Zuilhof, *Org. Lett.*, 2019, **21**, 3976.
24 X.-Y. Lou and Y.-W. Yang, *J. Am. Chem. Soc.*, 2021, **143**, 11976.
25 (*a*) M. L. Kaplan and W. D. Reents, *Tetrahedron Lett.*, 1982, **23**, 373; (*b*) J. Franke and F. Vögtle, *Tetrahedron Lett.*, 1984, **25**, 3445; (*c*) I. Baxter, H. M. Colquhoun, P. Hodge, F. H. Kohnke and D. J. Williams, *Chem. Commun.*, 1998, 283.
26 N. H. Park, G. dos Passos Gomes, M. Fevre, G. O. Jones, I. V. Alabugin and J. L. Hedrick, *Nat. Commun.*, 2017, **8**, 166.
27 E. V. Dalessandro and J. R. Pliego, *Theor. Chem. Acc.*, 2020, **139**, 27.
28 M. A. Spackman and D. Jayatilaka, *CrystEngComm*, 2009, **11**, 19.
29 H. Li, L. Li, R.-B. Lin, W. Zhou, Z. Zhang, S. Xiang and B. Chen, *EnergyChem*, 2019, **1**, 100006.
30 D. B. Hibberta and P. Thordarson, *Chem. Commun.*, 2016, **52**, 12792.